Towards the distributed burning regime in turbulent premixed flames

A. J. Aspden[1,2,†], M. S. Day[2] and J. B. Bell[2]

[1]School of Engineering, Newcastle University, Stephenson Building, Claremont Road, Newcastle upon
Tyne NE1 7RU, UK

[2]Center for Computational Sciences and Engineering, Lawrence Berkeley National Laboratory,
MS50A-3111, 1 Cyclotron Road, Berkeley, CA 94720, USA

Three-dimensional numerical simulations of canonical statistically steady, statistically
planar turbulent flames have been used in an attempt to produce distributed burning in
lean methane and hydrogen flames. Dilatation across the flame means that extremely
large Karlovitz numbers are required; even at the extreme levels of turbulence studied
(up to a Karlovitz number of 8767) distributed burning was only achieved in the
hydrogen case. In this case, turbulence was found to broaden the reaction zone
visually by around an order of magnitude, and thermodiffusive effects (typically
present for lean hydrogen flames) were not observed. In the preheat zone, the species
compositions differ considerably from those of one-dimensional flames based a
number of different transport models (mixture averaged, unity Lewis number and
a turbulent eddy viscosity model). The behaviour is a characteristic of turbulence
dominating non-unity Lewis number species transport, and the distinct limit is again
attributed to dilatation and its effect on the turbulence. Peak local reaction rates are
found to be lower in the distributed case than in the lower Karlovitz cases but higher
than in the laminar flame, which is attributed to effects that arise from the modified
fuel-temperature distribution that results from turbulent mixing dominating low Lewis
number thermodiffusive effects. Finally, approaches to achieve distributed burning at
realisable conditions are discussed; factors that increase the likelihood of realising
distributed burning are higher pressure, lower equivalence ratio, higher Lewis number
and lower reactant temperature.

Key words: combustion, flames, turbulent reacting flows

---

1. Introduction

The distributed burning regime of turbulent premixed flames represents the
limiting case where flame propagation is driven by turbulent mixing rather than
molecular diffusion (Aspden, Day & Bell 2011*b*), and corresponds to the small-scale
turbulence limit (Damköhler 1940; Peters 2000); the reader is referred to Aspden
et al. (2011*b*) for a more detailed review of the use of the term 'distributed

† Email address for correspondence: andrew.aspden@ncl.ac.uk

burning'. The feature that distinguishes burning in the distributed mode is that turbulent eddies comparable with the reaction zone thickness can mix faster than the flame can burn. Experimentally, there is some evidence of what will be referred to here as 'transitionally distributed' burning, particularly in high-speed piloted lean-to-stoichiometric methane jet flames; see, for example, Dunn *et al.* (2010), Zhou *et al.* (2017), Skiba *et al.* (2018) and the references therein. Previous numerical studies of transitionally distributed flames include Poludnenko & Oran (2010), Aspden *et al.* (2011*b*), Lapointe, Savard & Blanquart (2015), Savard & Blanquart (2015), Nilsson *et al.* (2018), Wang *et al.* (2018) and the references therein. All of these studies have demonstrated flames with broadened preheat zones, but none have shown broadening of the actual reaction zone by turbulence alone. Skiba *et al.* (2018) referred to this mode of burning as 'broadened preheat thin reactions'.

Distributed burning has been observed numerically in an astrophysical context (Aspden *et al.* 2008*a*), where a single-step reaction model was used to represent thermonuclear fusion in a type Ia supernova flame. Subsequently, Aspden, Bell & Woosley (2010) demonstrated scaling laws for distributed supernova flames following Damköhler (1940) and Peters (2000), along with the so-called 'λ-flame' regime; the combination of large Karlovitz and Damköhler numbers gives rise to flames simultaneously in the small-scale and large-scale limits. The resulting regime has such a large range of turbulent scales that the flame burns in the distributed mode, but the larger scales are unable to mix before the flame burns; this mode of burning aligns with that predicted by Zimont (1979) (which we argue requires the distributed transition to broaden the flame), and the local turbulent flame thickness λ corresponds to the Zimont length (Peters 2000) at that Karlovitz number. These supernova studies used an idealised configuration capable of subjecting the flame to arbitrary levels of turbulence favourable for distributed burning (the Reynolds number in a supernova can be in excess of 10^{10} and the Mach number around 10^{-5}); realisable conditions for distributed burning in terrestrial chemical flames are yet to be established.

In the present paper, lean premixed methane and hydrogen flames have been simulated with extreme levels of turbulence (root-mean-square (r.m.s.) velocity fluctuations exceeding four hundred times the laminar flame speed). At the highest turbulence levels, the hydrogen flame has been found to present substantial broadening of the reaction zone, but even with such intense turbulence, the methane flame did not. Despite the abstracted configuration and unrealistic conditions, this hydrogen flame represents the transition to distributed burning expected of a terrestrial chemical flame if suitable conditions can be contrived (i.e. at the same Karlovitz and Damköhler numbers). Phenomenological observations are first presented, followed by consideration of global consumption speeds, flame thickening, and conditional means of heat release and species mass fractions. The paper concludes with a discussion of the distributed burning regime and potential conditions required to realise distributed burning at realisable conditions.

1.1. *A note on Karlovitz number*

The classical Richardson/Kolmogorov picture of turbulence is a cascade of turbulent eddies from the energy-containing large scales through the inertial subrange to the dissipation subrange. If it is assumed that turbulence is sufficient for the inertial subrange to extend down to the flame scale, (equivalently, the flame is in the thin reaction zone, or the Karlovitz number is larger than unity), then as in the classical picture, there are energy-containing large scales responsible for the supply of kinetic

energy through the inertial subrange to the flame scale, where (unlike the non-reacting case) dilatation modifies the turbulent structure close to the flame before it reaches a classical dissipation subrange. Energy is still dissipated by viscosity at small scales, but not at the usual Kolmogorov length scale that would be expected in a constant-density flow; see Towery *et al.* (2016) for a more detailed consideration of energy spectra in premixed flames.

For this reason, it seems illogical to define the Karlovitz number (in the sense of being characteristic of turbulence–flame interaction at the flame scale) in terms of Kolmogorov scales; these scales simply are not representative of the physical processes taking place. Following the Kolmogorov similarity hypotheses, the universal equilibrium range is determined by the energy dissipation rate (ε) and viscosity (ν). The second similarity hypothesis gives rise to the inertial subrange independent from ν, determined solely by ε. This second hypothesis appears to be relevant to a turbulent premixed flame, which suggests a relevant dimensionless parameter can be defined as

$$\Pi_\varepsilon^2 = \frac{\varepsilon}{\varepsilon_F} = \frac{u'^3}{l}\frac{l_F}{s_F^3}, \tag{1.1}$$

where u' and l are the r.m.s. velocity fluctuation and integral length scale respectively, and s_F and l_F are the characteristic speed and thermal thickness of the flame (and $\varepsilon_F = s_F^3/l_F$). This quantity is the same as a more conventionally defined Karlovitz number based on the Kolmogorov time scale and by assuming a unity flame Reynolds number i.e. $s_F l_F = \nu$ (e.g. Peters 2000), but the argument here is that (1.1) is the appropriate dimensionless parameter that characterises the strength of turbulence at the flame scale in the thin reaction zone and above, (specifically, $u_F/s_F = \Pi_\varepsilon^{2/3}$, where u_F is the velocity associated with a turbulent eddy in the inertial subrange at the flame scale), and so should be considered the starting point, rather than resulting from any assumption. It is not only important to distinguish this quantity from the conventional definition involving Kolmogorov scales, but also from the definition used in the flamelet regimes as a measure of flame stretch; these definitions represent fundamentally different physical interactions. Despite the distinction, Π_ε will still be referred to here as a Karlovitz number (with $Ka \equiv \Pi_\varepsilon$) and the implicit understanding that it is not a measure of stretch, nor does it involve viscosity.

2. Simulation details

2.1. *Numerical solver*

The numerical solver used here is based on the well-established low Mach number formulation of the reacting flow equations (Day & Bell 2000; Nonaka *et al.* 2012). The fluid is treated as a mixture of perfect gases, and a mixture-averaged model is assumed for diffusive transport. A source term is used in the momentum equation to establish and maintain turbulence with the desired properties (Aspden *et al.* 2008*b*). The chemical kinetics and transport are modelled using the hydrogen mechanism of Li *et al.* (2004) consisting of 9 species with 21 fundamental reactions, and the GRIMech 3.0 methane mechanism (Frenklach *et al.* 1995) with the nitrogen reactions removed, resulting in 35 species and 217 reactions. These evolution equations are supplemented by CHEMKIN-compatible databases for thermodynamic quantities, and transport properties computed using EGLIB (Ern & Giovangigli 1996).

This solver is capable of running implicit large eddy simulation (ILES); non-oscillatory finite-volume schemes such as this are able to dissipate kinetic energy
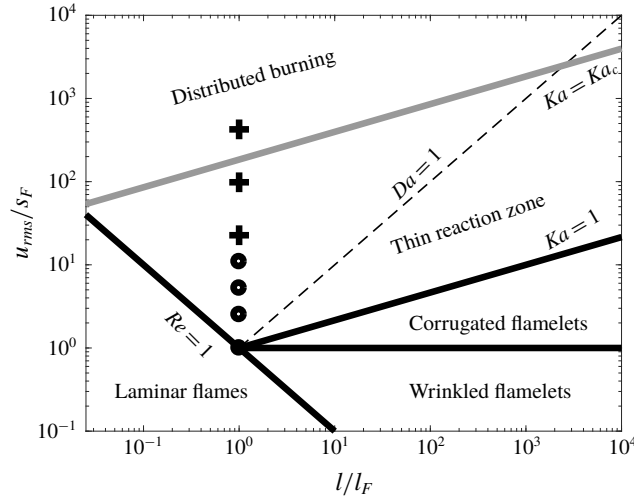
FIGURE 1. Turbulent premixed regime diagram showing the simulations in the present study (pluses) along with our previous simulations (circles) at lower *Ka* (Aspden *et al.* 2017); note that the critical Karlovitz number is shown in grey, and has been placed higher than is usual.

numerically at the grid scale in a stable and physical manner without resolving all the way down to the Kolmogorov length scale (see Grinstein, Margolin & Rider (2007) for a review). In the present simulations, especially at the highest turbulence intensities, there is some reliance on this ILES capability in that the Kolmogorov length scale in the reactants is not resolved on the grid. The performance of this solver in such under-resolved conditions was characterised in Aspden *et al.* (2008*b*), and further details are given below.

2.2. *Simulation configuration*

Following our previous studies (e.g. Aspden *et al.* 2011*b*; Aspden, Day & Bell 2015, 2016), a canonical periodic-box configuration was used, where a lean premixed flame was allowed to propagate through maintained zero-mean homogeneous isotropic turbulence. All simulations were run at atmospheric conditions in a high aspect ratio domain, with periodic lateral boundary conditions, a free-slip base and outflow at the top. Lean premixed hydrogen (equivalence ratio $\varphi = 0.4$, Lewis number $Le \approx 0.37$) and methane ($\varphi = 0.7$, $Le \approx 1.0$) were considered. The freely propagating hydrogen flame speed and thickness are $s_F = 0.474$ m s^{-1} and $l_F = 410$ µm; the laminar methane flame speed and thickness are $s_F = 0.189$ m s^{-1} and $l_F = 660$ µm. It was shown in Aspden *et al.* (2008*b*) that the forcing approach gives approximately 10 integral length scales across the domain width. In all cases the length scale ratio is $\Lambda = l/l_F = 1$, consistent with our previous studies (e.g. Aspden *et al.* (2017)). Three further Karlovitz numbers have been considered $Ka = 108$, 974 and 8767, which correspond to velocity ratios $\Upsilon = u'/s_F = 22.7$, 98.3 and 425, respectively. Present simulations and previous simulations are shown respectively as pluses and circles on a regime diagram in figure 1, where the critical Karlovitz number for transition to distributed burning has been shown in grey, and placed higher than is usual; it should be noted that this critical Karlovitz number is strongly dependent on the reactant conditions.

Case	CH$_4$ (108)	CH$_4$ (974)	CH$_4$ (8767)	H$_2$ (108)	H$_2$ (974)	H$_2$ (8767)
Υ	22.7	98.3	425	22.7	98.3	425
Ka	108	974	8767	108	974	8767
Da	0.0440	0.0102	0.00235	0.0440	0.0102	0.00235
Ka_η	285	2561	23 047	350	3149	28 339
Ka_{η_e}	257	1486	6955	289	1538	7012
Re	157	679	2938	237	1027	4442
Re_e	128	229	268	162	245	272

TABLE 1. Simulation parameters (based on reactant conditions).

Most simulations were conducted with a domain size of $10l_F \times 10l_F \times 80l_F$ discretised on a grid of $192 \times 192 \times 1536$ computational cells; the hydrogen case with the highest Ka required a larger domain ($10l_F \times 10l_F \times 120l_F$; $192 \times 192 \times 2304$ cells) to accommodate the growth of the flame brush. This resolution corresponds to 19.2 cells across a thermal thickness, which is more than sufficient to resolve these chemical mechanisms (Aspden *et al.* 2011*b*, 2016). At such high turbulence levels, the Kolmogorov length scale is between 44 and 544 times smaller than the thermal thickness of the flame; it is not resolved on this grid and so these simulations cannot be considered direct numerical simulation in the sense that the term implies well-resolved down to the Kolmogorov length scale. The effective Kolmogorov length scale (see Aspden *et al.* (2008*b*) for details) can be evaluated for this solver, and was found to range between 38 and 67 times smaller than the thermal thickness, which indicates that the turbulence that interacts with the flame (i.e. at the flame scale) is sufficiently well resolved (and is maintained by the momentum source term through the inertial cascade). Moreover, as previously argued, turbulence is strongly affected by dilatation, therefore, close to the flame, the Kolmogorov length is not the value that would be expected from the classical cascade; we argue that scales not represented on the grid have an inconsequential effect on burning regime and leading-order flame response to turbulence, and resolving them would be a waste of computational effort. The simulation parameters are given in table 1, where $Ka_\eta = t_F/t_\eta$ denotes the more conventional Karlovitz number as the ratio of flame time ($t_F = l_F/s_F$) to Kolmogorov times ($t_\eta = \eta/u_\eta$), $Re = u'l/\nu$ is the Reynolds number and the suffix e denotes effective quantities (i.e. using η_e and ν_e) evaluated following Aspden *et al.* (2008*b*); note that all values are based on reactant conditions.

To establish the consequences of this lack of resolution on the turbulence, simulations of non-reacting homogeneous isotropic turbulence have been run at four times the resolution extending the length scales at each end of the spectrum separately. These simulations are presented in appendix A and demonstrate that the use of maintained turbulence ensures the turbulence at the flame scale is the same as that that would have originated from a larger integral length scale at the same Karlovitz number (i.e. has the correct energy dissipation rate) despite the limited inertial subrange, and that the scales that are deficient are sufficiently smaller than the flame scale that we argue can be considered inconsequential. The effective Reynolds number is naturally lower, but the Karlovitz number (appropriately defined as above) is unaffected because the energy dissipation rate is unaffected by the lack of small-scale resolution. Note that it is this specific numerical approach (i.e. ILES capable) that means the apparent lack of resolution does not invalidate the results; approximately 20 computational cells across the flame thermal thickness is sufficient.

An additional simulation was also run to establish the consequences of under-resolving the Kolmogorov length scale in the methane case at $Ka = 8767$, which was achieved by adding a level of adaptive mesh refinement (AMR) and restarting a calculation from a steady-state check point (thereby having nearly 40 computational cells across the laminar thermal thickness); the results are presented in appendix B. The turbulent flame speed was found to be almost unchanged with increased resolution, conditional means of fuel consumption rate and heat release were indistinguishable between resolutions, but there were subtle differences between the thickening metric (based on temperature gradients). The higher resolution simulation lends further support to our argument that the turbulent scales that are not resolved on the grid are inconsequential as far as the flame physics is concerned.

It should be further stressed that these simulations are numerical experiments, and this set of values is not realisable experimentally; in particular, the low Mach number approximation is exploited here to preclude strong compressibility effects and prevent any potential detonation (e.g. Poludnenko & Oran 2010). Note in particular that the low Mach number approximation is not valid at these conditions; these simulations are not intended as a true representation of how these flames would respond, but how turbulent flames at the same Karlovitz and Damköhler numbers would respond if conditions could be constructed at low Mach number. Furthermore, viscous heating has not been included, which would have the potential to lead to a significant rise in reactant temperature as a result of continual energy injection by the momentum forcing term. Despite the limitations of this configuration, especially at the highest *Ka*, these simulations capture turbulence–flame interactions during the transition towards the limiting case of flame propagation driven by turbulent mixing, i.e. distributed burning, and are of significant interest and relevance to the transition away from the thin reaction zone with increasing levels of turbulence. Possible steps to realise distributed burning experimentally are discussed in § 4.

3. Results

3.1. *Flame response overview*

A general overview of flame response to high *Ka* turbulence is presented in figure 2, which depicts slices of fuel mass fraction, temperature, fuel consumption rate (FCR) and heat release rate (HR), normalised by the corresponding laminar values (note for hydrogen, the FCR and HR are normalised by ten times the laminar value to allow for the enhanced reaction rates due to the thermodiffusive instability).

Methane at $Ka = 108$ appears to be similar to moderate *Ka* (see the $Ka = 36$ case in Aspden *et al.* 2016); the flame surface is convoluted but smooth, generally similar to the laminar flame, with a decrease in reaction rates correlated with high positive curvature, which was attributed to atomic hydrogen diffusion (Echekki & Chen 1996; Aspden *et al.* 2016). The temperature field shows clear evidence of turbulent mixing, but restricted to the preheat region.

Methane at $Ka = 974$ continues the trend of increased turbulent mixing in the preheat region, but the reaction rates appear to be changing; while not immediately apparent in the image, the peak value exceeds the laminar flame values in places, and there appears to be greater variability along the flame surface, which is becoming more convoluted – again, this can be attributed to atomic hydrogen diffusion (Echekki & Chen 1996; Aspden *et al.* 2016).

Methane at $Ka = 8767$ shows different behaviour than the lower *Ka* cases; in addition to the mixing observed in the preheat region, there are indications in the
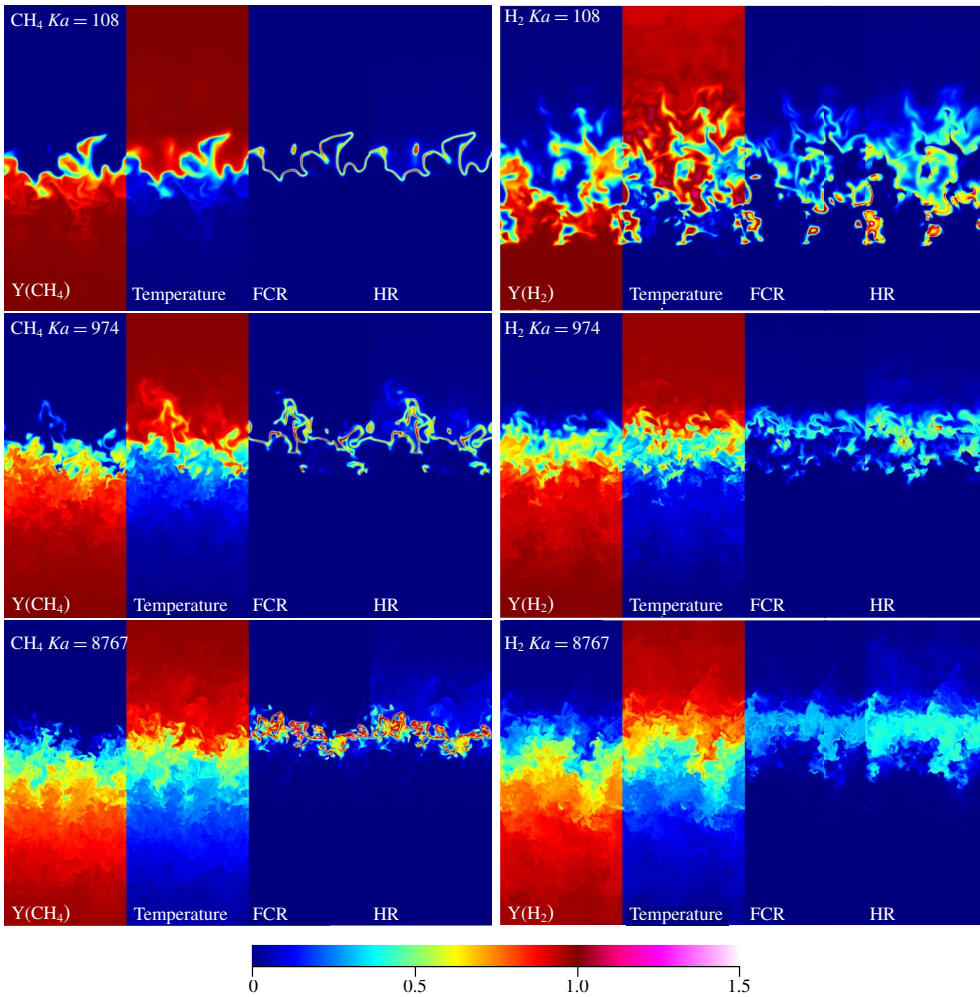
FIGURE 2. (Colour online) Slices of fuel mass fraction, temperature, fuel consumption rate and heat release for CH_4 and H_2 flames at $Ka = 108$, 974 and 8767, respectively. Each part of each panel shows $20l_F \times 50l_F$ (note that periodicity has been exploited to stitch together x–z and y–z planes to show more flame surface).

temperature field that there is an onset of turbulent mixing in the post-flame region. Interestingly, the reaction rates appear slightly increased in places (see magenta/white regions; an enlarged image is shown in figure 3), but are not broadened by turbulence.

Hydrogen at $Ka = 108$ presents significant thermodiffusively unstable behaviour (e.g. Baum *et al.* 1994; Trouvé & Poinsot 1994), and continues the trend from that observed in Aspden *et al.* (2011*b*, 2015); turbulence exaggerates the thermodiffusive instability, creating small-scale structures with higher curvature than at lower Ka, resulting in more intense burning over a broad flame brush (localised heat release rates in excess of fifteen times the laminar value are observed; shown by the white regions). The decorrelation between fuel consumption and heat release rates (reported by Chen & Im (2000) and Aspden *et al.* (2015), and demonstrated to be due to atomic hydrogen diffusion Aspden (2017)) is present, further indicating persistence
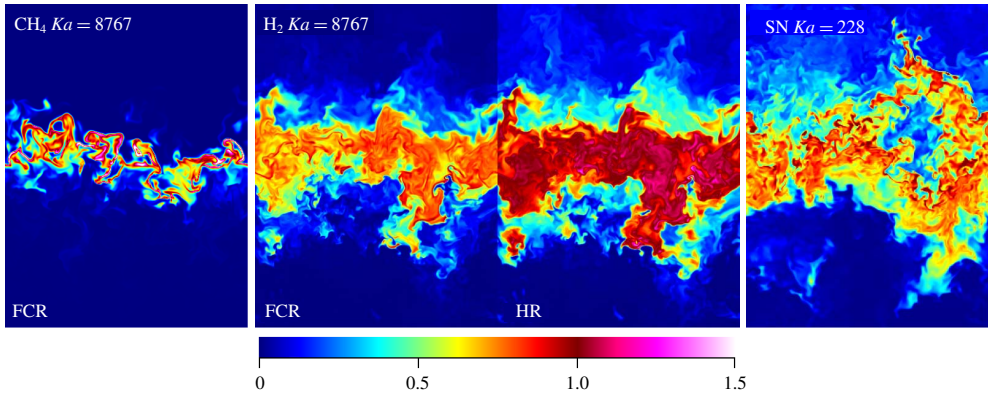
FIGURE 3. (Colour online) Slices of FCR for CH_4, and FCR and HR for H_2 at $Ka = 8767$ (each panel shows approximately $20l_F \times 30l_F$); for H_2 the normalisation is four times the laminar value (rather than ten). The reaction rate from the distributed supernova flame (Aspden *et al.* 2008*a*) is shown for comparison (the panel shows approximately $40l_F \times 60l_F$), which is normalised by one fifth of the corresponding laminar value.

of preferential diffusion at this Ka. Super-adiabatic temperatures still exist in the near post flame region. The temperature field presents limited turbulent mixing; the thermodiffusive instability leads to a resistance to turbulent mixing.

At $Ka = 974$, the hydrogen flame presents the first evidence of a change in behaviour; the thermodiffusively unstable structures at lower Ka are no longer observed, reaction rates have generally decreased, and the temperature field shows significant evidence of turbulent mixing in the preheat region.

At the highest Ka, the hydrogen flame presents significantly different behaviour to all of the other cases; there is now substantial turbulent mixing throughout the flame, there is no evidence of the thermodiffusive instability, the reaction rates are substantially lower than the other two hydrogen cases, and distributed relatively smoothly across a region that is over ten thermal thicknesses across. This behaviour is consistent with the distributed supernova flame presented in Aspden *et al.* (2008*a*); figure 3 reinforces this similarity by comparing the reaction rates from the distributed supernova flame with hydrogen fuel consumption rate and heat release (now normalised by four times the laminar values rather than ten). The peak reaction rates in the hydrogen case are lower than those of the moderate turbulent cases, but remain higher than in the one-dimensional laminar flame. This is in contrast to the supernova flame that showed a decrease in local fuel consumption rate; this can be explained as the suppression of Lewis number effects, and will be discussed further in §4.

3.2. *Turbulent flame speeds*

Turbulent flame speeds are shown both as a function of time and as a function of Ka in figure 4 (vertical lines in the latter denote the standard deviation after reaching a statistically steady state). Note that at such extreme levels of turbulence, tens of integral length eddy turnover times are required for the flame to reach a statistically steady state, and closer to 100 for the highest cases. The horizontal lines denote the mean and averaging period; in the following sections, all data has been temporally averaged in time using around 100 time points evenly distributed over the
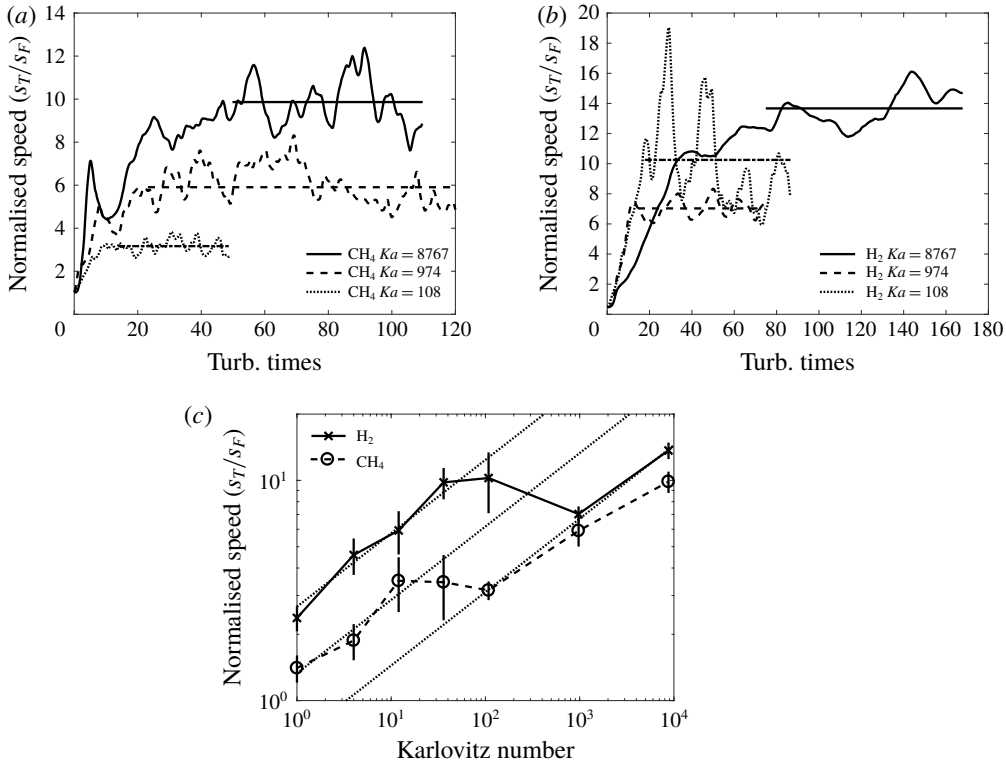
FIGURE 4. (*a*,*b*) Normalised turbulent flame speeds s_T/s_F as a function of turbulent eddy turnover times for methane (*a*) and hydrogen (*b*); horizontal lines denote the average and period treated as steady state. (*c*) Normalised turbulent flame speed as a function of *Ka*; the vertical lines show one standard deviation about the mean, and the dotted lines show the scaling $s_T/s_F \propto Ka^{1/3}$ (for fixed Λ), with three different constants of proportionality.

corresponding time periods. Power law scaling (as a function of *Ka*) can be derived in analogy with Damköhler (1940) for the distributed limit of turbulence-driven mixing, which is shown by the dotted lines (see also Peters (2000)). Predicting a turbulent flame speed $s_T = \sqrt{D_T/\tau_T}$, where $D_T = \alpha u' l$, is a turbulent diffusion for some constant α and (turbulent) chemical time scale τ_T (both to be determined), three equivalent expressions can be derived

$$\frac{s_T}{s_F} \propto \Lambda^{2/3}\, Ka^{1/3}, \quad \frac{s_T}{s_F} \propto \Lambda\, Da^{-1/2}, \quad \text{or} \quad \frac{s_T}{s_F} \propto \Lambda^{1/2}\, \Upsilon^{1/2}, \qquad (3.1a\text{--}c)$$

where the constant of proportionality in all three cases is $\alpha^{1/2} Da_T^{-1/2}$; note the latter can be written as $(Re/Re_F)^{1/2}$ for $Re_F = s_F l_F/\nu$. It is as yet unclear why both hydrogen and methane flames appear to follow this scaling law in a regime where it is not intended to apply (other than a simple dimensional necessity) followed by an apparent transition, after which the flame speeds may again follow the scaling law, especially since distributed burning behaviour is only observed for hydrogen at $Ka = 8767$. It should be borne in mind that the present measure of turbulent flame speed is a global-consumption-based metric, and will depend on the size of the domain (which is usually not considered). Extending the domain without changing
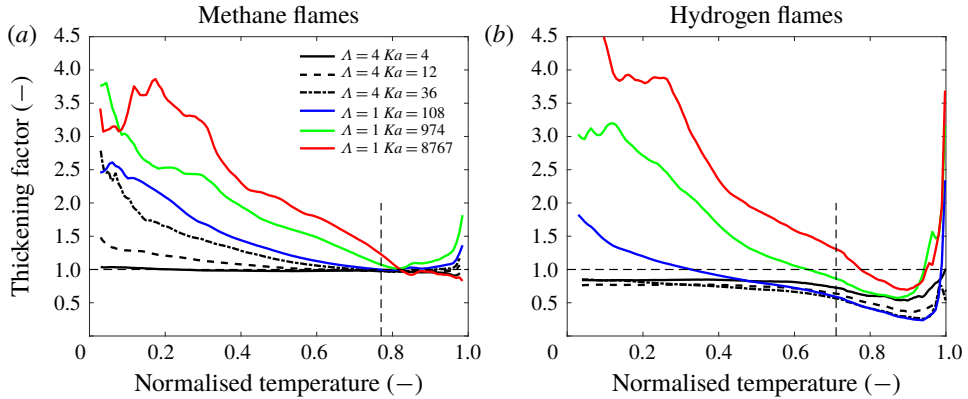
FIGURE 5. (Colour online) Thickening factor $\Theta(T)$ for CH_4 (*a*) and H_2 (*b*) compared with previous lower Ka cases from Aspden *et al.* (2015, 2016), which are shown in black.

the integral length scale is unlikely to result in a simple periodic replica of the present flame; there is a greater volume into which the flame can develop, leading to greater flame surface area, and therefore greater turbulent flame speed by the present global-consumption-based metric.

3.3. *Thickening factor*

A local thickening factor was previously defined (Aspden *et al.* 2016) analogously to thermal thickness as the ratio of the conditional means of temperature gradients as

$$\Theta_n(T) = \frac{\langle \nabla T(\xi) \mid \xi = T \rangle_{Ka=1}}{\langle \nabla T(\xi) \mid \xi = T \rangle_{Ka=n}}, \tag{3.2}$$

where the normalisation by the conditional mean at $Ka = 1$ is used (in preference to the laminar profile) to account for the thermodiffusive instability in the hydrogen flames. In that paper, the methane flames were shown to be broadened in the preheat region, unlike the hydrogen flames, which became progressively thinner with increasing Ka due to generation of more highly curved flame surface by turbulence thereby enhancing the thermodiffusive effects. The thickening factor in the present flames are compared in figure 5 with these previous lower Ka cases; the methane flames are broadened further in the preheat region with increasing Ka, but seem to remain thin at $Ka = 8767$ in the post-flame region (the vertical dashed line indicates the location of peak HR). The thinning trend in hydrogen is reversed in the preheat region at higher Ka, but remain thinner in the post-flame region. This thinning in the post-flame region may be due in part to the normalisation, where the temperature profile $Ka = 1$ flame (as for the laminar flame) has a long tail at high temperatures (i.e. small gradients), resulting in a smaller Θ due a modified post-flame structure at high Ka. Furthermore, it appears that the thickening factor does not reflect the visual thickening observed in figure 2; as the turbulence intensity increases, the flame becomes less flamelet-like, turbulent mixing maintains strong local gradients distributed over a broad region in space, which is compounded by conditioning on temperature without accounting for the broadening of the temperature field itself.
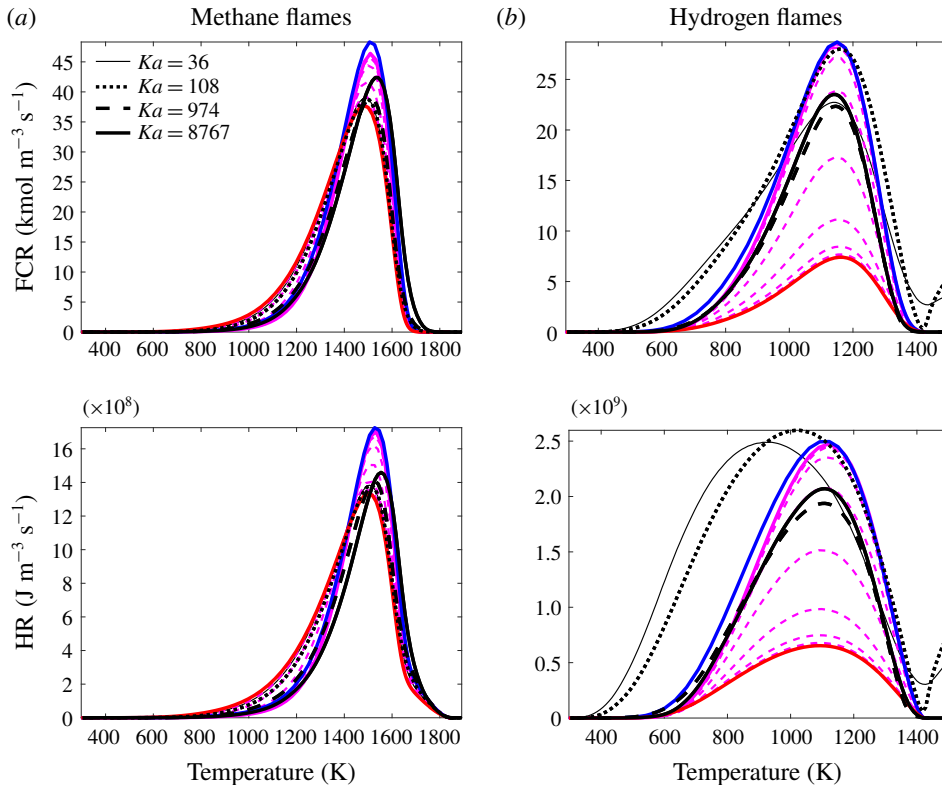
FIGURE 6. (Colour online) Conditional means of fuel consumption rate and heat release for CH_4 (*a,c*) and H_2 (*b,d*) flames. Black lines are the conditional means from the simulations, red is the one-dimensional laminar flame profile, blue is the one-dimensional unity Lewis number profile and the dashed magenta lines are one-dimensional laminar flames with an added turbulent diffusion of increasing magnitude with the limiting case shown as a solid line.

At the highest *Ka*, this metric becomes less reliable in the preheat region due to resolution limitations; the simulation with refined computational grid demonstrates that this sensitivity is predominantly observed in the preheat region, but is slight in the region of the flame (see figure 12 in appendix B).

3.4. *Reaction rates*

The response of reaction rates to turbulence is considered using conditional means of fuel consumption rate and heat release rate in figure 6. One-dimensional flame solutions are also presented for comparison: the red line denotes the laminar flame and the blue line denotes the unity Lewis number flame. The dashed magenta lines were obtained by one-dimensional calculations of the laminar flame where each diffusion coefficient has been supplemented by a constant turbulent diffusion (i.e. the diffusion coefficient D_i for species i was increased by D_T, where D_T is a turbulent diffusion coefficient, with a corresponding thermal term to ensure unity Lewis number of the supplementary terms); D_T was gradually increased in magnitude (giving the different dashed magenta lines) until the profile stopped changing, and that limiting case is shown by the solid magenta line.

At low-to-moderate *Ka*, the methane profile is close to the laminar profile, but at the highest *Ka* the profile appears to have shifted toward higher temperatures, with a slight increase in peak magnitude (consistent with figure 2). A more pronounced response is observed in the hydrogen flames; at low-to-moderate *Ka*, there is substantial heat release rate in the preheat region (due to the thermodiffusive instability exaggerated by moderate turbulence), whereas at higher *Ka* the distribution is narrower, with a peak that again has shifted to higher temperatures, consistent with the peak temperature in the one-dimensional profiles, again indicative of suppression of Lewis number effects. Importantly, note the similarity between the hydrogen flames at $Ka = 974$ and 8767; this suggests that the conditional mean is tending to a limiting distribution, which we argue is to be anticipated as a characteristic of distributed burning.

3.5. *Species mass fraction distributions*

For the methane flames, the turbulent response of conditional means of species mass fractions remain consistent with the classification set out in Aspden *et al.* (2016); figure 7(*a,c,e*) presents conditional means of mass fractions for CH_4, H_2 and H_2O_2 at $Ka = 8767$ (conditional means for all species and *Ka* are provided as supplementary material, available at https://doi.org/10.1017/jfm.2019.316). The fuel distribution is close to linear for all profiles, but there is the suggestion that the turbulent profile is slightly higher than the one-dimensional profiles (not seen in the lower *Ka* cases). The other two species present a strong response in the preheat region; specifically, turbulence dominates species diffusion at high *Ka*. The standard deviation decreases with *Ka*, and the distribution not only transitions from that comparable with the laminar profile (red) towards the unity Lewis number profile (blue), but also appears to reach a state that is distinct from all three of the one-dimensional profiles. Aspden *et al.* (2016) suggested that a temperature-dependent diffusion coefficient may account for the difference, and that it may be due the effect of dilatation on turbulence through the flame; there may also be a change in chemical time scale. Other species with distributions notably distinct are C_2H_2, HCCOH and CO (see supplementary material).

A similar response is found for intermediate species in the hydrogen flames, but there is a significantly different response in the fuel distribution; figure 7(*b,d,f*) presents conditional means of species mass fraction for H_2, H and H_2O_2 at $Ka = 8767$. The fuel distribution has moved away from the (low *Le*) one-dimensional laminar flame (that lies below the diagonal) towards the unity Lewis number profile that aligns with the diagonal mixing line. The response of H is characteristic of O and OH (again, all species are presented as supplementary material), where the enhanced radical pool at low-to-moderate temperatures observed at lower *Ka* (see Aspden *et al.* 2015, and supplementary material) is suppressed at $Ka = 8767$. A strong response of H_2O_2 is observed in the preheat region, and again appears to tend to a limit distinct from the three one-dimensional profiles. The standard deviation is also significantly reduced, almost to zero.

4. Discussion and conclusions

Numerical simulations at extreme levels of turbulence have shown a transition to distributed burning in lean premixed hydrogen flames. The phenomenology of the transition is similar to that reported in an astrophysical context (Aspden *et al.* 2008*a*); there are no indications that suggest other fuels should not undergo a similar transition at sufficiently intense turbulence levels. Unrealistically high turbulence conditions were required to observe the transition, which is argued to be primarily
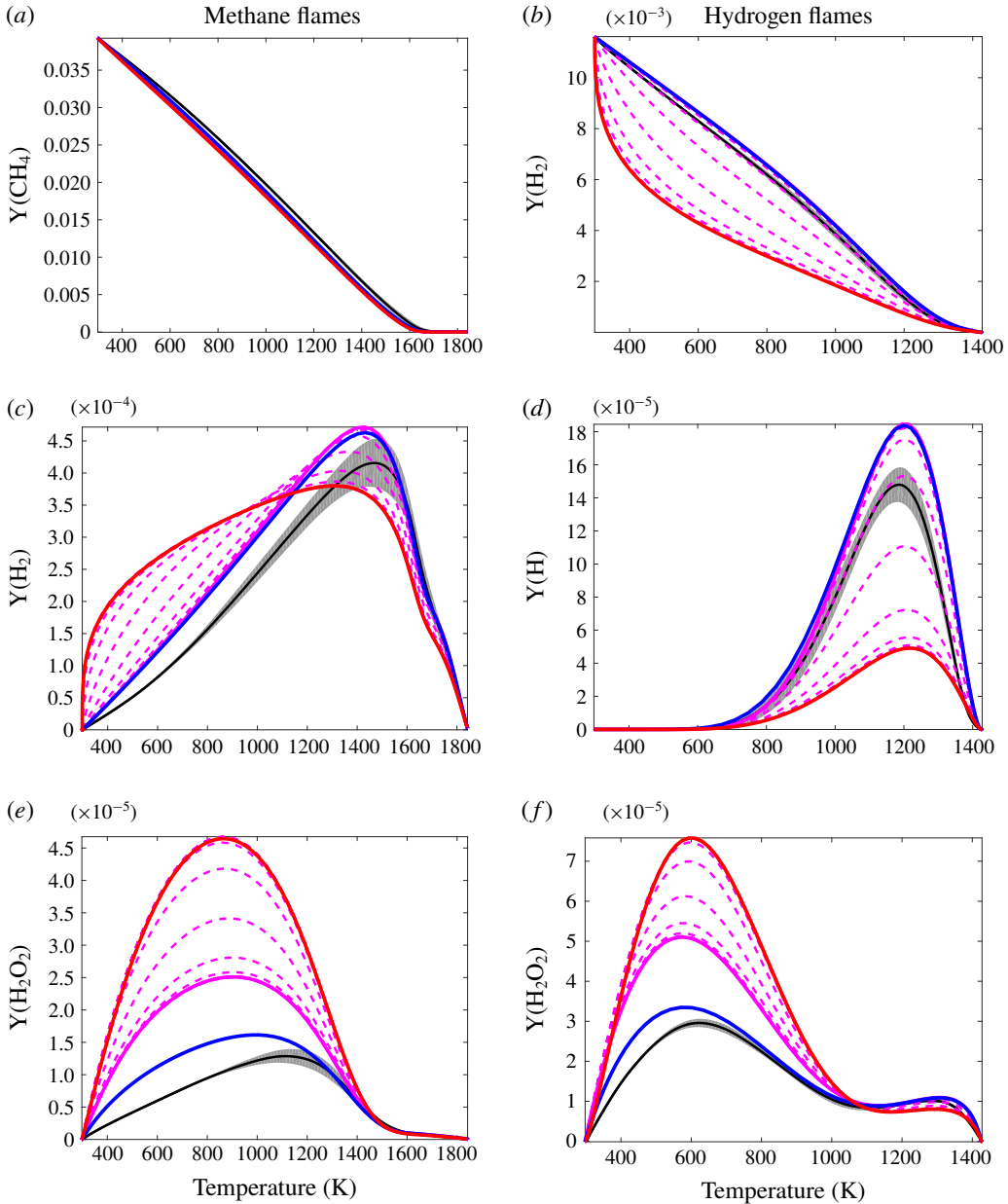
FIGURE 7. (Colour online) Conditional means of species mass fraction for CH$_4$ (*a,c,e*) and H$_2$ (*b,d,f*) flames at *Ka* = 8767; see figure 6 for a description of the line styles, with the addition of one standard deviation about the mean shown in grey.

due to dilatation and the higher density ratio between unburned and burned conditions (the density ratio is less than two for the supernova case, about four for hydrogen, and over six for methane); this effect was not observed in constant-density reaction wave propagation by Yu & Lipatnikov (2017), for example. The effect of density ratio may also be compounded by the thickness of the reaction zone relative to the
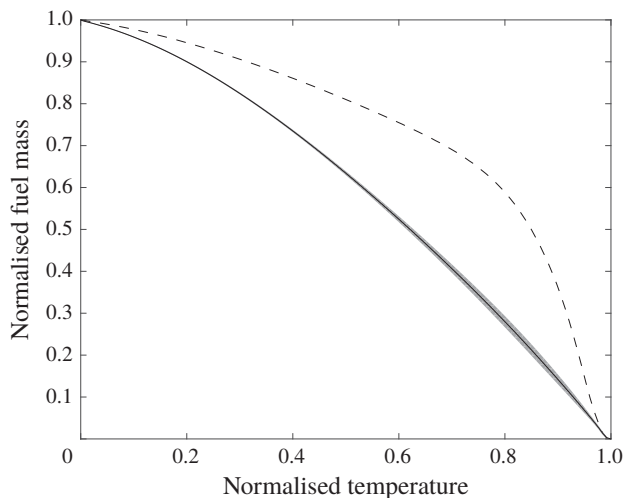
FIGURE 8. Conditional mean of normalised fuel mass from the distributed supernova flame at $Ka = 266$ (Aspden *et al.* 2008*a*); the conditional mean is the solid line with one standard deviation in grey, and the laminar flame profile is shown by the dashed line.

thermal thickness; the reaction thickness in the methane flame is relatively narrower than in the hydrogen flame, so turbulence has to survive deeper into the methane flame to disrupt the reaction zone.

The key behaviour characteristic of distributed burning not previously observed in chemical flames is broadening of the reaction zone by turbulence; here, the heat release region was visually found to be broadened by around an order of magnitude. Thermodiffusive effects (in particular, the super-adiabatic regions and the decorrelation of FCR and HR) were found to be suppressed, if not eliminated, with the peak reaction rates falling from about fifteen times the peak laminar value to about four times. Distributed reaction rates that are higher than the corresponding laminar flame is different from the response found in the supernova flame, where the peak reaction rates were found to be much smaller. This can be attributed to global Lewis number by considering the fuel-temperature distribution, as discussed in Aspden, Day & Bell (2011*a*). Hydrogen has a low Lewis number, and so the fuel-temperature distribution of the laminar flame lies below the linear mixing distribution. Strong turbulent mixing gives an effective unity Lewis number for all species (species and enthalpy are advected together in packets) so the distributed flame profile is close to linear – fuel concentrations are higher at the same temperature, so reaction rates and heat release increase. Conversely, for the supernova, the Lewis number is large, so the laminar flame profile lies above the linear mixing distribution (see figure 8), and turbulent mixing results in fuel concentrations that are lower at the same temperature, giving lower reaction rates.

Turbulent flame speeds were found to follow scaling laws at low-to-moderate Karlovitz numbers (despite not satisfying the assumptions made), followed by an apparent transition. Even at the extreme turbulence levels considered, there was insufficient evidence to draw solid conclusions about behaviour in the distributed burning regime, and will require significant further work to demonstrate the behaviour observed in the supernova flames (Aspden *et al.* 2010).
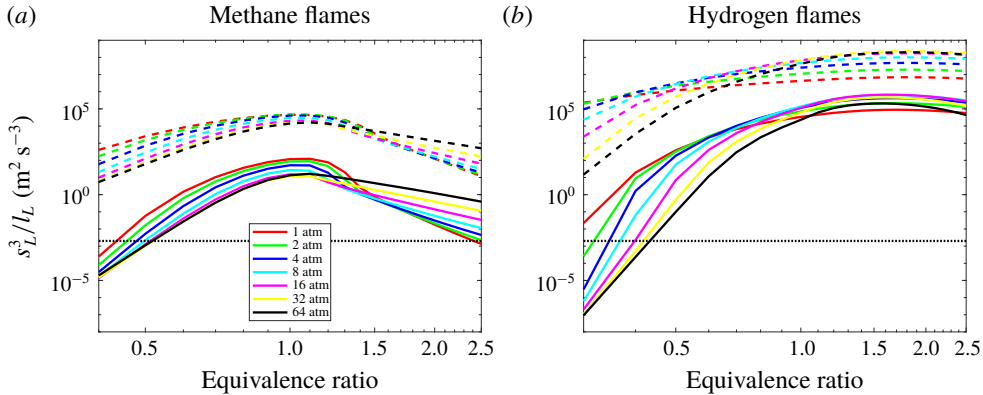
FIGURE 9. (Colour online) Laminar flame properties from methane (*a*) and hydrogen (*b*) flames; solid and dashed lines denote reactant temperatures of 300 K and 800 K, respectively. Maximising Karlovitz number is equivalent to minimising s_L^3/l_L; given sample conditions of $u' = 10$ m s^{-1} at $l = 5$ mm, a Karlovitz number in excess of 10 000 can be achieved for reactant conditions with s_L^3/l_L below 0.002 m^2 s^{-3}, as shown by the dotted horizontal line.

The species distribution tends towards a limit that is distinct from the one-dimensional profiles (laminar, unity *Le* and turbulent diffusive limit), with a standard deviation of almost zero; Aspden *et al.* (2016) suggested that a temperature-dependent diffusion coefficient is required to account for dilatation through the flame. A change in distribution was observed in particular for species that experience low-temperature activity (e.g. H_2O_2), which is argued to result from molecular diffusion of mobile species such as H_2 and/or H being overcome by turbulent mixing.

4.1. *Transition to distributed burning*

We continue to interpret the distributed burning regime as the limiting behaviour where turbulent mixing dominates species and thermal diffusion to drive flame propagation, as discussed in Aspden *et al.* (2011*b*), along with the consequences described therein. It is well established that turbulence increases the flame surface area and exaggerates the thermodiffusive instability, but once turbulence is sufficiently intense, it can overcome dilatation effects to disrupt the reaction zone. We posit that the turbulently mixed flame structure (i.e. chemical distribution and reaction rates conditioned on some measure of progress variable such as temperature) eventually reaches a limiting state (distinct from other one-dimensional distributions considered here) that is invariant under further increases in turbulent intensity. The turbulent flame speed and thickness will respond to such increases in turbulent intensity (and so spatial gradients will eventually become small) but the underlying flame structure will not change (in temperature space).

We argue that only turbulence–flame interactions around the flame scales, i.e. length scales comparable with the thermal and reaction thicknesses, are relevant to the transition; larger scales serve to move the turbulent flame structure around, and smaller scales are not dynamically important. Therefore, the relevant dimensionless quantity necessary for distributed burning is sufficiently high Karlovitz number, defined according to (1.1), because it appropriately characterises the turbulence in

terms of the inertial subrange. As Karlovitz number increases, turbulence is able to penetrate further into the flame, until eventually it is sufficiently strong enough to overcome dilatation effects and mix the reaction zone quicker than it can burn. While these simulations have a particularly small integral length scale, they are representative of how turbulence at the same Karlovitz number would interact with the flame; the response to increasing the integral length scales at a fixed Karlovitz number in the distributed regime was demonstrated in Aspden *et al.* (2010), consistent with Zimont (1979).

The critical Karlovitz number necessary is fuel dependent, and will be higher where the density jump across the flame is large (due to suppression of turbulence by dilatation); it is not universal, and it is certainly not 100. The global Lewis number (that of the deficient species) will also affect this critical Karlovitz number. The transition to distributed burning increases the local reaction rates for low *Le* (and *vice versa* for high *Le*), which suggests that the critical Karlovitz number required to transition will be lower at high *Le*; if the reaction rates decrease, then there is more time for turbulence to interact with the reaction zone, allowing it to mix before it can burn. Moreover, the Karlovitz number defined in (1.1) is based on the laminar flame properties (or indeed freely propagating values in the case of hydrogen), but in a distributed flame, the global Lewis number becomes irrelevant because molecular diffusion is dominated by turbulent mixing; if one were to artificially alter the global Lewis number, the reference flame properties would be different, but the corresponding distributed flames should be anticipated to be identical for the same turbulence conditions (not the same *Ka*). This suggests that the critical Karlovitz number could be evaluated based on a one-dimensional calculation that somehow accounts for the subtle interaction of an appropriate turbulent mixing model (with an effectively unity Lewis number) and the resulting chemical time scale. Furthermore, the use of the freely propagating reference values may only be relevant for the thin reaction zone.

We contend that the present hydrogen flame at the highest *Ka* has indeed achieved the distributed burning regime. Note that the limiting case is not confirmed definitively by the present simulations as that would require yet higher *Ka* to establish invariant behaviour (although the $Ka = 974$ case is not substantially different). What is confirmed by the present simulations is a change in flame structure, especially a spatial broadening of the reaction zone by turbulence, accompanied by a (*Le*-dependent) change in magnitude, and a distinct chemical distribution.

4.2. *Potential for realising distributed burning*

Whether or not there is a practical use for distributed flames remains to be seen, but it remains a phenomenon of academic interest, in particular as the limiting case of high Karlovitz number turbulence–flame interaction. The conditions required here for distributed burning are unphysical and unrealisable in practice, but there are steps that could be taken that may lead to distributed burning. To explore potential conditions, a series of one-dimensional laminar flame calculations were run using Cantera (Goodwin *et al.* 2018) to obtain the laminar flame speed (s_L), the thermal thickness (l_L) and the density ratio ($P = \rho_u/\rho_b$) between reactant and products. Reactant temperatures were varied between 300 and 800 K, pressures from 1 to 64 atm, and equivalence ratios from 0.3 for H_2 and 0.4 for CH_4 (and $C_{12}H_{26}$; see supplementary material) up to 2.5.

Since the strength of the turbulence that interacts at the flame scale depends solely on Ka, then for given turbulence conditions u' and l, finding reactant conditions favourable for distributed burning (i.e. maximising Ka) is equivalent to minimising s_L^3/l_L. Starting with example realisable conditions, say $u' = 10$ m s^{-1} at $l = 5$ mm, then obtaining a Karlovitz number of 10 000 requires the ratio s_L^3/l_L to be below 0.002 m^2 s^{-3}. This ratio is shown for methane and hydrogen flames as a function of equivalence ratio at $T = 300$ K (solid lines) and 800 K (dashed lines) for all pressures (all other data is presented as supplementary material). Figure 9 shows that the likelihood of realising distributed burning can be increased by increasing pressure, decreasing equivalence ratio, and decreasing reactant temperature. Preheating reduces the density ratio, and therefore the impact of dilatation on turbulence through the flame, but increasing the reactant temperature from 300 to 800 K only reduces the density ratio by a factor of about two. The increase in flame speed is closer to two orders of magnitude, and so is likely to far outweigh the benefit of reduced density ratio; preheating is unlikely to be favourable for the transition to distributed burning.

Supplementary material

Supplementary material is available at https://doi.org/10.1017/jfm.2019.316.

Appendix A

To explore the potential consequences of the lack of resolution on the turbulence, this appendix presents simulations of homogeneous isotropic turbulence in a triply periodic cube at the same (reactant) conditions as the hydrogen flame case at the highest Karlovitz number. One simulation was run at 192^3, corresponding directly to the same resolution as the flame simulation, another at 768^3 with the same integral length scale and therefore four times the resolution, and a final case at 768^3 with an integral length scale four times greater (denoted $4l$) and therefore matching the cell size; in this last case, the magnitude of the forcing was increased to match the energy dissipation rate, which corresponds to matching the Karlovitz number.

The kinetic energy density spectra for the three cases are shown in figure 10(a), where the wavenumber has been normalised by the laminar flame thickness and the energy density has been normalised by that at the flame scale in the 192^3 case. Note the coincidence of the inertial subranges, however short, and that they closely follow the expected five-thirds cascade. The inertial subrange of the 192^3 case is clearly truncated by the lack of small-scale resolution, however this occurs at wavenumbers greater than the flame scale, which supports the argument that the scales represented on the grid are adequate to capture turbulence–flame interactions. The energy density spectra have also been recast schematically on the regime diagram by noting $\sqrt{\kappa E}$ is representative of the velocity scale, where κ and E are wavenumber and energy density, respectively. This illustrates how the inertial subrange follows a constant Karlovitz line (shown by the dashed black line; referred to as turbulence
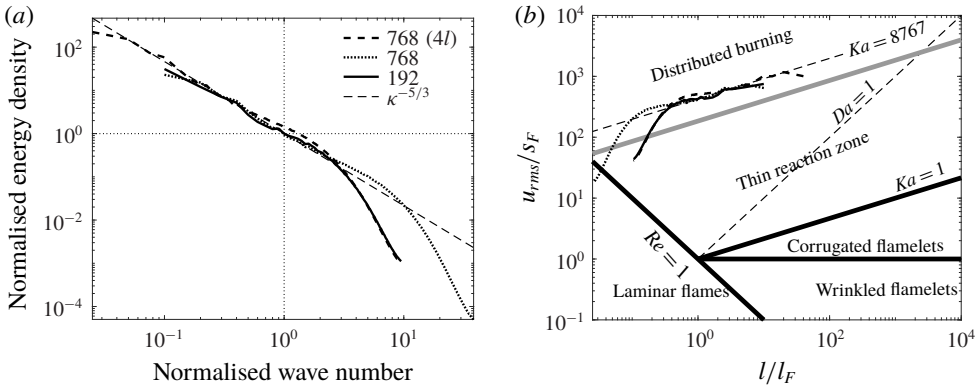
FIGURE 10. Normalised kinetic energy density spectrum as a function of wavenumber normalised by the thermal thickness of the laminar flame (*a*), and the same recast schematically on the regime diagram (*b*).

lines by Poinsot & Veynante (2005), for example) because the energy dissipation rate is constant throughout ($Ka \sim \varepsilon^{1/2} \sim$ const.), and where the lack of resolution compromises the calculation (the inertial range should continue to follow the constant Karlovitz line), again lending support to the argument that the lack of resolution will not be detrimental to resolving the flame physics. It is this coincidence of the inertial subrange with the constant Karlovitz line that supports the use of so-called small eddy simulation approach for turbulence–flame interactions, and for the use of the present definition of *Ka* (rather than one involving Kolmogorov scales or viscosity); specifically, it is the appropriate definition characterising turbulence–flame interactions, not one based on the Kolmogorov time scale and the assumption that $\nu \approx s_F l_F$. The simulations presented here are underresolved, which leads to a smaller effective Reynolds number but the Karlovitz number (appropriately defined) is the same.

Appendix B

To establish the consequences for not completely resolving the spatial scales down to the Kolmogorov length scale in the methane flame at the highest Karlovitz number, this appendix presents an additional simulation with higher resolution; this was achieved by restarting the calculation with one level of adaptive mesh refinement around the flame. Refinement was added based on formaldehyde mole fraction (above 5×10^{-4}) with an additional buffer of 16 computational cells, following Aspden *et al.* (2011*b*) to allow the higher wavenumbers to become populated; at this higher resolution there are over 38 computational cells across the thermal thickness of the laminar flame.

Figure 11 shows slices of fuel, temperature, fuel consumption rate and heat release for the case with adaptive mesh refinement (for comparison with figure 2), along with formaldehyde mole fraction with the gridding threshold contour shown in black and the resulting region of increase resolution shown by the two white lines. While it is unreasonable to expect that the turbulence structure is exactly the same, the general flame features appear unaffected by the increase in resolution.

Figure 12 shows normalised turbulent flame speed, thickening factor and conditional means of fuel consumption rate and heat release (conditioned on temperature); in each
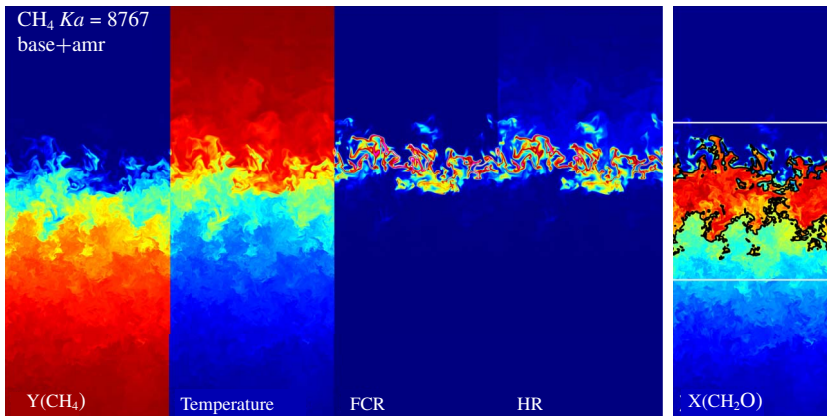
FIGURE 11. (Colour online) Slices of fuel mass fraction, temperature, fuel consumption rate and heat release for the CH_4 flame at $Ka = 8767$ run with adaptive mesh refinement (for comparison with figure 2), along with formaldehyde mole fraction, which was used for gridding criterion (the black contour plus a 16-cell buffer resulted in the region between the two horizontal white lines being refined, capturing the reaction layer and a substantial region ahead of it).
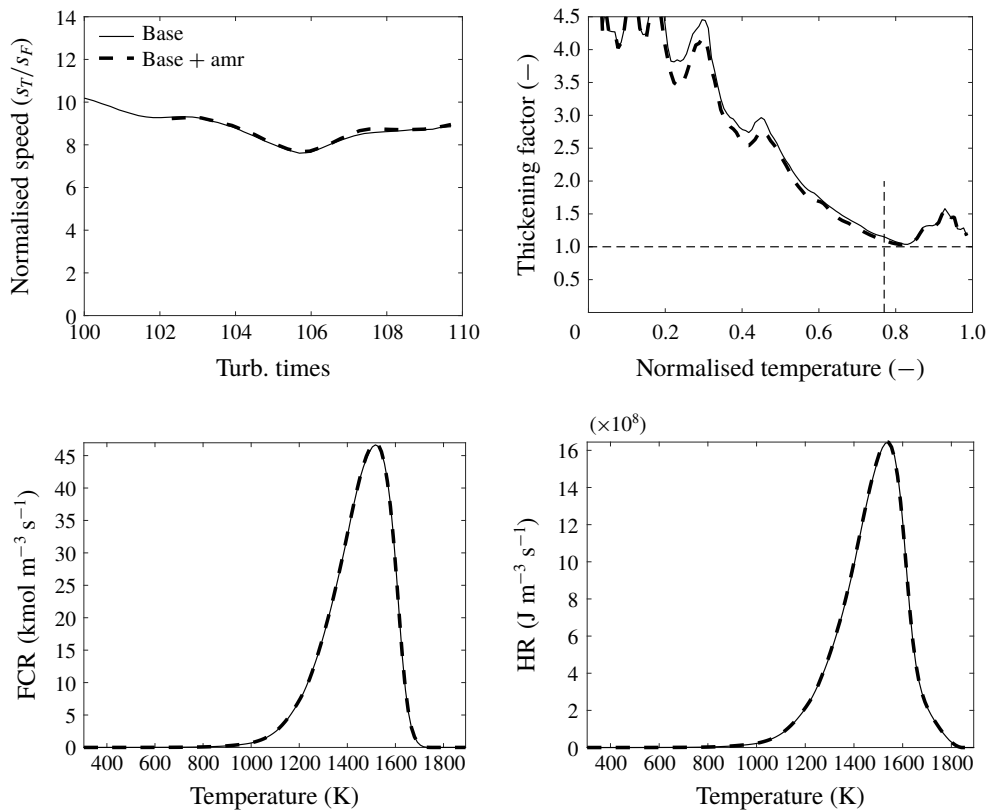

FIGURE 12. Comparison of turbulent flame speeds, thickening factor and conditional means of fuel consumption rate and heat release with adaptive mesh refinement for the CH_4 flame at $Ka = 8767$.

case, the base grid is shown as a thin solid line, and the case with adaptive mesh refinement is shown as a thick dashed line. The temporal averaging was performed over the final two thirds of the restarted run (corresponding to about five eddy turnover times), and the same time period was also used at the lower resolution. The turbulent flame speed (a global metric) agrees almost exactly between resolutions, and the conditional means of fuel consumption rate and heat release (local metrics) are indistinguishable. There do appear to be differences in the thickening factor between the two resolutions, specifically, the thickening factor is lower at the higher resolution, indicative of slightly higher gradients; both the higher gradient and disparity are not particularly surprising, especially for a higher moment in a short period of temporal averaging. Ultimately, this higher resolution simulation demonstrates that the effect of the apparent lack of resolution is small.

REFERENCES

ASPDEN, A. J. 2017 A numerical study of diffusive effects in turbulent lean premixed hydrogen flames. *Proc. Combust. Inst.* **36**, 1997–2004.

ASPDEN, A. J., BELL, J. B., DAY, M. S. & EGOLFOPOULOS, F. N. 2017 Turbulence–flame interactions in lean premixed dodecane flames. *Proc. Combust. Inst.* **36**, 2005–2016.

ASPDEN, A. J., BELL, J. B., DAY, M. S., WOOSLEY, S. E. & ZINGALE, M. 2008*a* Turbulence–flame interactions in type Ia supernovae. *Astrophys. J.* **689**, 1173–1185.

ASPDEN, A. J., BELL, J. B. & WOOSLEY, S. E. 2010 Distributed flames in type Ia supernovae. *Astrophys. J.* **710**, 1654–1663.

ASPDEN, A. J., DAY, M. S. & BELL, J. B. 2011*a* Lewis number effects in distributed flames. *Proc. Combust. Inst.* **33** (1), 1473–1480.

ASPDEN, A. J., DAY, M. S. & BELL, J. B. 2011*b* Turbulence–flame interactions in lean premixed hydrogen: transition to the distributed burning regime. *J. Fluid Mech.* **680**, 287–320.

ASPDEN, A. J., DAY, M. S. & BELL, J. B. 2015 Turbulence–chemistry interaction in lean premixed hydrogen combustion. *Proc. Combust. Inst.* **35** (2), 1321–1329.

ASPDEN, A. J., DAY, M. S. & BELL, J. B. 2016 Three-dimensional direct numerical simulation of turbulent lean premixed methane combustion with detailed kinetics. *Combust. Flame* **166**, 266–283.

ASPDEN, A. J., NIKIFORAKIS, N., DALZIEL, S. B. & BELL, J. B. 2008 Analysis of implicit LES methods. *Commun. Appl. Maths Comput. Sci.* **3** (1), 101–126.

BAUM, M., POINSOT, T. J., HAWORTH, D. C. & DARABIHA, N. 1994 Direct numerical simulation of $H_2/O_2/N_2$ flames with complex chemistry in two-dimensional turbulent flows. *J. Fluid Mech.* **281**, 1–32.

CHEN, J. H. & IM, H. 2000 Stretch effects on the burning velocity of turbulent premixed hydrogen/air flames. *Proc. Combust. Inst.* **28** (1), 211–218.

DAMKÖHLER, G. 1940 Der Einfluss der Turbulenz auf die Flammengeschwindigkeit in Gasgemischen. *Z. Elektrochem.* **46**, 601–652.

DAY, M. S. & BELL, J. B. 2000 Numerical simulation of laminar reacting flows with complex chemistry. *Combust. Theor. Model.* **4**, 535–556.

DUNN, M. J., MASRI, A. R., BILGER, R. W. & BARLOW, R. S. 2010 Finite rate chemistry effects in highly sheared turbulent premixed flames. *Flow Turbul. Combust.* **85** (3–4), 621–648.

ECHEKKI, T. & CHEN, J. H. 1996 Unsteady strain rate and curvature effects in turbulent premixed methane-air flames. *Combust. Flame* **106** (1–2), 184–202.

ERN, A. & GIOVANGIGLI, V. 1996 Optimized transport algorithms for flame codes. *Combust. Sci. Technol.* **118**, 387–396; see also http://www.cmap.polytechnique.fr/www.eglib/.

FRENKLACH, M., WANG, H., GOLDENBERG, M., SMITH, G. P., GOLDEN, D. M., BOWMAN, C. T., HANSON, R. K., GARDINER, W. C. & LISSIANSKI, V. 1995 GRI-Mech – an optimized detailed chemical reaction mechanism for methane combustion. *Tech. Rep.* GRI-95/0058. Gas Research Institute, http://www.me.berkeley.edu/gri_mech/.

GOODWIN, D. G., SPETH, R. L., MOFFAT, H. K. & WEBER, B. W. 2018 Cantera: An object-oriented software toolkit for chemical kinetics, thermodynamics, and transport processes. Version 2.4.0. Available at: http://www.cantera.org.

GRINSTEIN, F. F., MARGOLIN, L. G. & RIDER, W. J. 2007 *Implicit Large Eddy Simulation*. Cambridge University Press.

LAPOINTE, S., SAVARD, B. & BLANQUART, G. 2015 Differential diffusion effects, distributed burning, and local extinctions in high Karlovitz premixed flames. *Combust. Flame* **162** (9), 3341–3355.

LI, J., ZHAO, Z., KAZAKOV, A. & DRYER, F. L. 2004 An updated comprehensive kinetic model of hydrogen combustion. *Intl J. Chem. Kinet.* **36** (10), 566–575.

NILSSON, T., CARLSSON, H., YU, R. & BAI, X.-S. 2018 Structures of turbulent premixed flames in the high Karlovitz number regime – DNS analysis. *Fuel* **216**, 627–638.

NONAKA, A., BELL, J. B., DAY, M. S., GILET, C., ALMGREN, A. S. & MINION, M. L. 2012 A deferred correction strategy for low mach number flow with complex chemistry. *Combust. Theor. Model.* **16** (6), 1053–1088.

PETERS, N. 2000 *Turbulent Combustion*. Cambridge University Press.

POINSOT, T. & VEYNANTE, D. 2005 *Theoretical and Numerical Combustion*, 2nd edn. Edwards.

POLUDNENKO, A. Y. & ORAN, E. S. 2010 The interaction of high-speed turbulence with flames: global properties and internal flame structure. *Combust. Flame* **157** (5), 995–1011.

SAVARD, B. & BLANQUART, G. 2015 Broken reaction zone and differential diffusion effects in high Karlovitz n-C_7H_{16} premixed turbulent flames. *Combust. Flame* **162** (5), 2020–2033.

SKIBA, A. W., WABEL, T. M., CARTER, C. D., HAMMACK, S. D., TEMME, J. E. & DRISCOLL, J. F. 2018 Premixed flames subjected to extreme levels of turbulence part I: flame structure and a new measured regime diagram. *Combust. Flame* **189**, 407–432.

TOWERY, C. A. Z., POLUDNENKO, A. Y., URZAY, J., O'BRIEN, J., IHME, M. & HAMLINGTON, P. E. 2016 Spectral kinetic energy transfer in turbulent premixed reacting flows. *Phys. Rev.* E **93** (5), 053115.

TROUVÉ, A. & POINSOT, T. 1994 The evolution equation for the flame surface density in turbulent premixed combustion. *J. Fluid Mech.* **278**, 1–31.

WANG, H., HAWKES, E. R., SAVARD, B. & CHEN, J. H. 2018 Direct numerical simulation of a high Ka CH_4/air stratified premixed jet flame. *Combust. Flame* **193**, 229–245.

YU, R. & LIPATNIKOV, A. N. 2017 Direct numerical simulation study of statistically stationary propagation of a reaction wave in homogeneous turbulence. *Phys. Rev.* E **95** (6), 063101.

ZHOU, B., BRACKMANN, C., WANG, Z., LI, Z., RICHTER, M., ALDÉN, M. & BAI, X.-S. 2017 Thin reaction zone and distributed reaction zone regimes in turbulent premixed methane/air flames: scalar distributions and correlations. *Combust. Flame* **175**, 220–236.

ZIMONT, V. L. 1979 Theory of turbulent combustion of a homogeneous fuel mixture at high Reynolds numbers. *Combust. Explos. Shock Waves* **15** (3), 305–311.